Check for updates

AGU100 ADVANCING EARTH AND SPACE SCIENCE

Geophysical Research Letters

RESEARCH LETTER
10.1029/2019GL083783

Tropical Cyclone Cold Wake Size and Its Applications to Power Dissipation and Ocean Heat Uptake Estimates

Jishi Zhang[1], Yanluan Lin[1], Daniel R. Chavas[2], and Wei Mei[3]

[1]Ministry of Education Key Laboratory for Earth System Modeling, Department of Earth System Science, Tsinghua University, Beijing, China, [2]Department of Earth, Atmospheric, and Planetary Sciences, Purdue University, West Lafayette, IN, USA, [3]Department of Marine Sciences, University of North Carolina at Chapel Hill, Chapel Hill, NC, USA

Abstract Mixing of the upper ocean by the wind field associated with tropical cyclones (TCs) creates observable cold wakes in sea surface temperature and may potentially influence ocean heat uptake. The relationship between cold wake size and storm size, however, has yet to be explored. Here we apply two objective methods to observed daily sea surface temperature data to quantify the size of TC-induced cold wakes. The obtained cold wake sizes agree well with the TC sizes estimated from the QuikSCAT-R wind field database with a correlation coefficient of 0.51 and 0.59, respectively. Furthermore, our new estimate of the total cooling that incorporates the variations in the cold wake size provides improved estimates of TC power dissipation and TC-induced ocean heat uptake. This study thus highlights the importance of cold wake size in evaluating the climatological effects of TCs.

Plain Language Summary The wind field of a tropical cyclone can mix warm water downward, leaving a cold wake at the surface. This effect may influence ocean heat uptake within the climate system. We derive a novel oceanic metric of tropical cyclone size based on its induced cold wake using sea surface temperature data for a period from 2002 to 2011. The cold wake size agrees well with the wind field size determined from QuikSCAT surface winds. Furthermore, with the cold wake size incorporated, total cooling provides better quantifications of tropical cyclone power dissipation and cyclone-induced ocean heat uptake. More reliable estimates of cyclone power dissipation and sea surface cooling may be useful for both understanding and forecasting impacts of tropical cyclones on the climate system.

Key Points:
- The size of the tropical cyclone wind field correlates reasonably well with the size of its mixing-induced cold wake
- With the cold wake size incorporated, TC-induced sea surface total cooling has a better correspondence with TC power dissipation
- Compared to sea surface cooling with a fixed cold wake area, the total cooling provides an improved estimate of TC-induced ocean heat uptake

Supporting Information:
- Supporting Information S1

Correspondence to:
Y. Lin,
yanluan@tsinghua.edu.cn

Citation:
Zhang, J., Lin, Y., Chavas, D. R., & Mei, W. (2019). Tropical cyclone cold wake size and its applications to power dissipation and ocean heat uptake estimates. *Geophysical Research Letters*, *46*, 10,177–10,185. https://doi.org/10.1029/2019GL083783

Received 20 MAY 2019
Accepted 15 AUG 2019
Accepted article online 19 AUG 2019
Published online 30 AUG 2019
Corrected 17 AUG 2020

This article was corrected on 17 AUG 2020. See the end of the full text for details.

©2019. American Geophysical Union. All Rights Reserved.

1. Introduction

Tropical cyclones (TCs) not only can cause significant societal impacts but may also play a larger-scale role within the climate system by altering the distribution of sea surface temperatures (SSTs) and heat within the upper ocean (Emanuel, 2001; Fedorov et al., 2010; Mei et al., 2013; Sriver et al., 2010; Sriver & Huber, 2007). Specifically, the near-surface wind field of a TC drives vigorous mixing that stirs the stratified upper ocean. The resulting downward heat transfer generates prominent cold and warm anomalies, respectively, in the surface and subsurface layers, with the cold anomaly at the surface commonly referred to as the "cold wake". Direct surface-to-atmosphere heat loss contributes a small fraction of the cooling in the surface layer (e.g., Price, 1981; Vincent, Lengaigne, Madec, et al., 2012). The cold anomaly in the surface layer decays within a month or so, largely attributed to reduced sea-to-air heat fluxes (Mei & Pasquero, 2012), whereas part of the subsurface warm anomaly typically persists more than one year (Pasquero & Emanuel, 2008). These processes produce a net warming in the upper ocean a few months after the TC passage.

In addition to the fact that the magnitude of the cold wake can be closely related to the intensity of the TC, the size of the cold wake might be also closely related to the size of TC wind field. In this sense, the cold wake size can thus provide another measurement of TC size and broaden our understanding of their impacts on the climate. TC size, in addition to TC intensity, has been found to be vital to TC intensification and TC-induced damage in recent years (Carrasco et al., 2014; Chavas et al., 2013; Guo & Tan, 2017; Knutson et al., 2015; Lin & Chavas, 2012; Xu & Wang, 2015). Almost all current size metrics of TCs, however, are derived from atmospheric features, such as wind, sea level pressure, rainfall, and clouds (Chavas et al., 2016; Chavas & Emanuel, 2010; Kimball & Mulekar, 2004; Knaff et al., 2014; Lin et al., 2015; Merrill, 1984). An oceanic size metric of TCs has been absent to date.

The determination of cold wake size has many potential applications, including estimation of TC power dissipation and TC-induced ocean heat uptake. The knowledge of the cold wake size may be helpful for the estimation of TC wind power dissipation that characterizes the strength of the TC forcing for upper ocean mixing. Conventionally, TC wind power dissipation is calculated using the maximum wind speed rather than two-dimensional surface winds because of a lack of observations of the complete near-surface wind field (e.g., Emanuel, 2005). To remedy the deficiency in this method, area-integrated cold wake or total SST cooling has been proposed as a proxy of TC power dissipation since the kinetic energy input by TCs into the surface ocean is mostly used to generate vertical mixing and thereby ocean surface cooling (Vincent, Lengaigne, Vialard, et al., 2012). Excluding details in the cold wake size, however, may reduce the accuracy of this new methodology.

On the other hand, since the majority of the surface-layer cooling is caused by a downward heat transfer into the subsurface, the effect of TC-induced heat pumping can be better quantified after characterizing the magnitude, horizontal extent (i.e., the size of the cold wake), and depth of the cooling. Several studies have been devoted to such a quantification (Li et al., 2016; Park et al., 2011; Sriver et al., 2008; Sriver & Huber, 2007). All these studies, however, used a fixed value to represent the varying sizes of cold wakes, which introduces errors in assessing the heat pumping effect.

In this study, we apply two objective processing methods to daily SST fields to determine the size of the cold wakes and compare it with TC size computed using the QuikSCAT-R wind data—an effort that to the best of our knowledge has never been made. We then use the total cooling (i.e., cooling within the cold wake boundary) to evaluate how the inclusion of variations in cold wake size may affect the quantification of TC power dissipation and TC-induced ocean heat uptake.

2. Data and Method

To derive TC-generated SST anomalies (SSTAs), we use the daily NOAA 1/4° Optimum Interpolation Sea Surface Temperature, from which AVHRR + AMSR data sets (2002–2011) are adopted because of their lower uncertainty under clouds and higher spatial coverage over the open ocean (Reynolds et al., 2007). We also analyze a longer climatology based on AVHRR-only data sets (1981–2017). Global 6-hr TC location and intensity are extracted from the International Best Track Archive for Climate Stewardship (IBTrACS) version 3 (Knapp et al., 2010). Following previous work, we define TC wind field size as the azimuthally averaged radius of 12-m/s wind (hereafter "r12"; Chavas et al., 2016) from the QuikSCAT-R surface wind data set (1999–2009). To match the daily SST data, IBTrACS data at 00 UTC and the daily-averaged r12 are adopted since the r12 data are not standardized at 00 UTC. The power dissipation of TCs is derived from the Cross-Calibrated Multi-Platform (CCMP) gridded surface vector winds (Atlas et al., 2011). Monthly vertical temperature profiles (2002–2010) based on Coupled Ocean Data Assimilation of Zhang et al. (2007) are used to estimate TC-induced ocean heat uptake. The time period is 2002–2011 for the determination of cold wake size and the estimate of TC power dissipation, 2002–2010 for the estimate of TC-induced ocean heat uptake, and 2002–2009 for the comparison between cold wake size and r12.

2.1. TC-Induced Cold Wake Detection

In addition to TC-induced surface cooling, SSTs are also affected by mesoscale eddies and fronts in the ocean. To minimize the impact of oceanic eddies, a low-pass filter with a spatial scale of $2° \times 2°$, which covers a typical size of oceanic mesoscale eddies (Chelton et al., 2007), is applied to isolate the signals of TC-induced cold wakes. We also test the results using filters of $1° \times 1°$, $3° \times 3°$, and $4° \times 4°$, and obtain similar results. Overall, compared to the $2° \times 2°$ filter, the $4° \times 4°$ ($1° \times 1°$) filter makes the mean of cold wake sizes ~11% larger (~9% smaller; see Table S1). After filtering out oceanic eddies, those SSTAs are assumed to be induced principally by TCs.

To identify the SST cooling fields associated with each TC, we define SST perturbations as the difference between the SST 2 days after the TC passage and the mean SST for 3 to 10 days before the passage within a $30° \times 30°$ box centering at each TC center, following Lloyd and Vecchi (2011) and Vincent, Lengaigne, Vialard, et al. (2012). Note that the cold wake does not necessarily correspond to the TC wind structure instantaneously because it takes time for ocean mixing and other processes to occur. The cooling maximum is generally observed 0–5 days after the TC passage and the cooling usually persists for a month or so (Dare &

McBride, 2011; Mei & Pasquero, 2013). As a result, a banded cold wake along the track is prominent, especially for fast-moving TCs (Figures 1a and 1b), which reflects the movement of TC. The results are not sensitive to the choice of time after the TC passage (e.g., day 0, +1, +3, and average-day +1 to +3). Finally, tropical depressions and samples with the TC center less than 3° from the coast are excluded. Our final sample size is 7,038 SST snapshots associated with 906 storms.

2.2. Cold Wake Size Determination

Two methods are applied to the SSTA data to objectively determine the cold wake size. The first method is based on a region of interest (ROI) image processing algorithm (Lin et al., 2015), which accounts for persistence and asymmetries in the cold wake spatial distribution by determining its most appropriate boundary. Key parameters to identify the ROI are (1) a threshold value of SSTA (−0.7 °C) to mask the SSTA field where only SSTAs below this threshold are accounted, which is used to identify the ROIs, and (2) a tolerance distance with a radius of 6° from the TC center to exclude those ROIs far away from the TC center. The first criterion is chosen following Wang et al. (2016), who showed that the cold wake region is hardly distinctive from the background in regions where SSTAs are warmer than −0.5 ~−0.8 °C. A larger tolerance distance (11°) reduces the mean of ROI size slightly (<5%; see Table S2). The reason for this counterintuitive result can be found in Figure S3 and Text S3. The ability to remove small noisy warm patches is one of the key benefits of the ROI method. To facilitate a direct comparison with the cold wake size determined using the second method (described below) and r12, the surface area within the ROI boundary (S_{ROI}) is obtained by summing all the pixel area ($dx{\cdot}dy$), and then converted to an equivalent radius, rROI, using $\pi \cdot \mathrm{rROI}^2 = S_{ROI}$. rROI is thus an equivalent radius of the surface area of the ROI. Examples of raw ROI boundaries and equivalent radius are shown in Figure 1.

The second method (POLAR) assumes that the cold wake is axisymmetric and estimates cold wake radius in polar coordinates. First, the SSTA field is converted to a polar projection centered at the TC center and azimuthally averaged SSTA is calculated at 1/8° intervals. Then the cold wake radius, rPOL, is determined based on two criteria: (1) averaged SSTA smaller than a threshold value of −0.7 °C and (2) the radial gradient of averaged SSTA <0.05 °C per 1/8°. In general, TC-induced SST cooling decreases quickly away from the wake center, and thus, the latter criterion differentiates TC cold wake from other nearby anomalies. This method is less sensitive to spatial heterogeneity.

Three examples are shown in Figure 1 to illustrate these two methods. Overall, rROIs and rPOLs are in good agreement, and further, the ROI boundary can capture the asymmetry of wake region (e.g., Figures 1a–1d). The two methods produce the most similar results when the cold wake area is large (Figures 1e and 1f) or TCs move slowly (Figures 1f and 1i). Fast-moving TCs tend to leave elongated cold wakes, and in these cases, rROIs are generally larger than rPOLs.

3. Results

3.1. Comparison of Cold Wake Size With r12

Both rROI and rPOL compare reasonably well with r12 (Figures 2a and 2b) with a correlation coefficient of 0.51 and 0.59, respectively. Note that each size has been normalized by its mean. The choice of parameters in the ROI and POLAR methods mainly affect the absolute value of the cold wake sizes but not their correlations with r12. For example, a smaller SSTA threshold or a smaller tolerant distance would give a larger rROI. It is worth noting that when AVHRR-only Optimum Interpolation Sea Surface Temperature data set is used for the same period, the correlation of the cold wake size with r12 decreases significantly to 0.38 and 0.39, respectively. This suggests that high-quality SST data sets, that is, those having Microwave Scanning Radiometer (AMSR-E) measurements incorporated, are vital to determining the cold wake size.

Despite the significant correlations among rROI, rPOL, and r12, large discrepancies exist for some cases. rROI is larger than rPOL when TCs move quickly (see Text S1 and Figure S1), in line with the examples shown in Figure 1. In addition, deeper mixed-layer or weaker stratification favors smaller rPOL compared with r12, possibly resulting from weaker strength of cold wake (Lloyd & Vecchi, 2011; Vincent, Lengaigne, Vialard, et al., 2012; Wang et al., 2016). Note that the contributions of translation speed and vertical

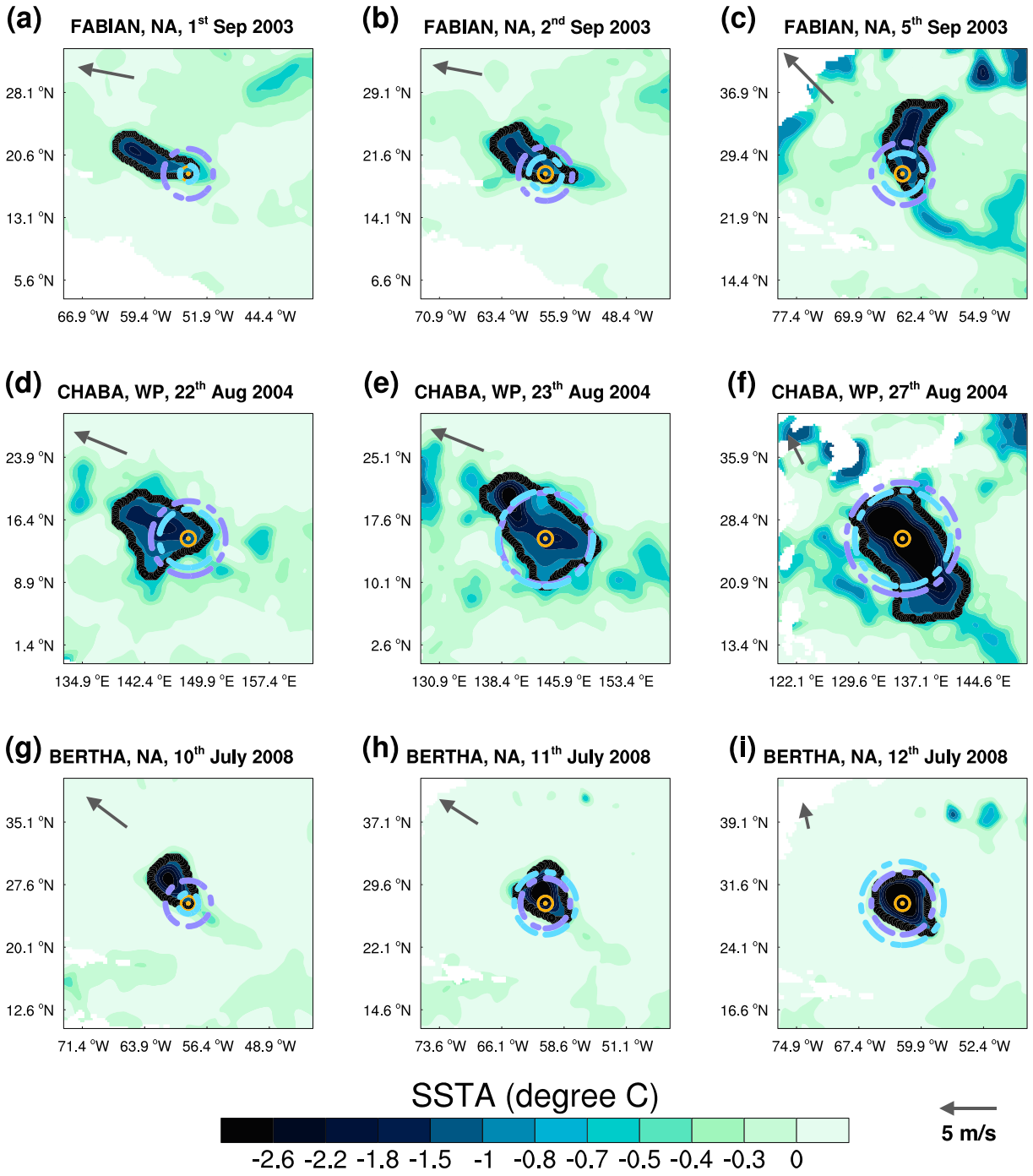

Figure 1. Examples of the cold wakes (°C; shaded) and their size based on the ROI and POLAR methods for (a–c) tropical cyclone Fabian in North Atlantic, (d–f) Chaba in Western Pacific, and (g–i) Bertha in North Atlantic. The ROI boundary is shown as the black thick line and an equivalent radius to represent the ROI size is shown as the purple dot-dashed circle. Sky-blue dot-dashed circles indicate the POLAR sizes. TC center is denoted by an orange circle-dot. The movement of TC is indicated by the gray arrow with a reference translation speed of 5 m/s at the bottom right corner.

temperature structure in the upper ocean to the discrepancies between cold wake sizes and r12 are rather small. In fact, multiple linear regression analyses suggest that inclusion of these factors only slightly increases the explained variance (not shown).

Globally, the spatial distributions of cold wake sizes and r12 are similar (Figure 3). They are the largest in the western/South Pacific, followed by the North Atlantic and Indian Ocean, and the smallest in the eastern Pacific. In addition, cold wake sizes tend to increase more with latitude than r12 in the western Pacific

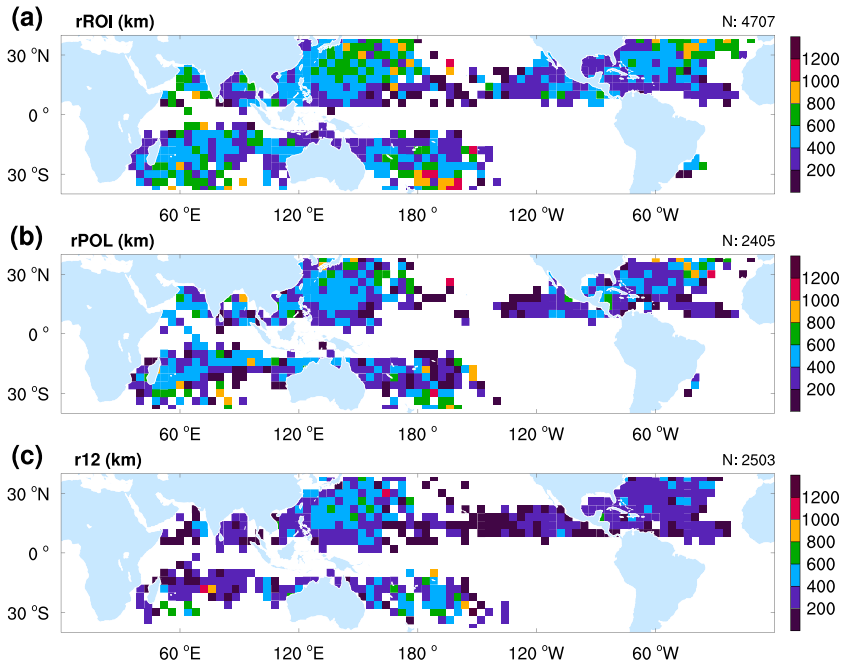

Figure 2. Global TC size (km) distribution of (a) the average cold wake size determined by the ROI method in every 4° × 4° box. (b and c) Same as (a) but for the POLAR method and r12 wind size from QuikSCAT-R. Sample sizes are denoted in the right top of each figure.

and North Atlantic where the midlatitude storms become increasingly prevalent. This may also be related to the decrease in climatological mixed-layer depth with latitude over the TC active regions (de Boyer Montégut, 2004).

3.2. Total Cooling as a Proxy of TC Power Dissipation

In an idealized framework, Vincent, Lengaigne, Vialard, et al. (2012) demonstrated that the TC-induced surface cooling is scaled to the cube root of the potential energy increase in a water column. This potential energy increase is related to the kinetic energy transferred by the storm to the upper ocean, which is highly related to the TC power dissipation (PD; Emanuel, 2005). Vincent, Lengaigne, Vialard, et al. (2012) calculated PD within 200 km of the TC center and found that it can approximate the total work of surface wind stress on the ocean. Following Vincent, Lengaigne, Vialard, et al. (2012), a local PD is derived from the fixed-domain integral of CCMP wind power within 200 km of the TC center. Similarly, a local SST cooling is

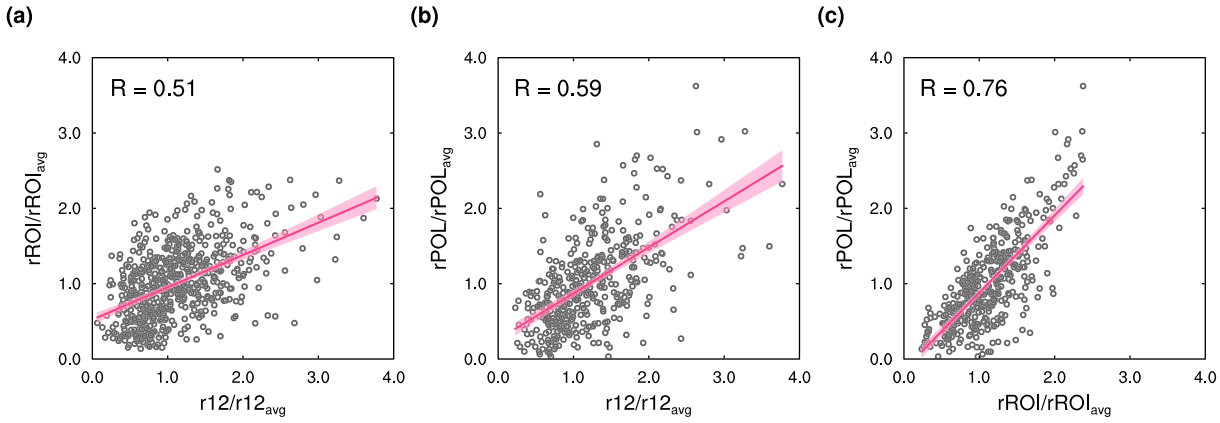

Figure 3. (a) Scatterplot of TC sizes between those derived from cold wake using the ROI method (rROI) and r12. (b) Same as (a) but for the sizes from the POLAR method (rPOL) and r12. (c) Scatterplot of rROI and rPOL. All sizes are normalized by their means, respectively. Correlation coefficient is shown in the top left corner. Linear regression fits are denoted as dark pink lines with two-sided 95% confidence bounds of the slopes shaded in pink.

defined as the area integral of SSTAs within the same domain. Similar to Vincent, Lengaigne, Vialard, et al. (2012), a good correspondence with a correlation coefficient of 0.62 between the two is noted. On the other hand, with the cold wake size known, the total cooling, defined as the area integral of the SSTAs and PD within the cold wake boundaries determined using the ROI method, can be computed. Similarly, the total PD is computed within a boundary of winds greater than 12 m/s using the CCMP wind field. By so doing, the effect of storm size is explicitly included in estimating both cold wake and PD.

The new size metrics provide a better quantification of TC-induced total cooling, which agrees well with TC PD. The correlation coefficient between the total cooling and the cube root of total PD reaches 0.56 (Figure 4a), larger than that between the local SST cooling and the cube root of total PD (0.49; Figure 4b). Note that the CCMP data set tends to underestimate the high wind speeds within the inner core of TCs owing to rain contamination (Ricciardulli & Wentz, 2015). Therefore, a merged wind field combining the CCMP winds with a Holland vortex (Holland, 1980) following Sun et al. (2015) and Zhang and Oey (2018) is alternatively tested. Note that the Holland vortex uses the maximum surface wind speed from IBTrACS and a parameterized radius of maximum wind based on Knaff et al. (2007) (see Text S2 and Figure S2). Based on the new wind field, correlation coefficient also increases when using the total cooling rather than the local cooling. This suggests the importance of accounting for cold wake area in addition to its cooling magnitude in estimating the total TC power dissipation.

3.3. A New Estimate of TC-Induced Ocean Heat Uptake

TC-induced change in ocean heat content is estimated following previous studies (Emanuel, 2001; Li et al., 2016; Sriver et al., 2008; Sriver & Huber, 2007): $Q = \iiint F\rho C\Delta T dh dW dL$. F was calculated to be 0.56 in Vincent, Lengaigne, Madec, et al. (2012) and 0.53–0.55 in a more recent study (Li et al., 2016) after considering the proportion of surface cooling due to enthalpy fluxes. The density and heat capacity of seawater ρ and C are 1,020 kg/m^3 and 3,900 J (kg °C)$^{-1}$, respectively. ΔT is the magnitude of surface cooling, dW is the cross-track width and dL is the along-track length, and dh is the depth of cooling layer, which is approximated as $\Delta T \cdot \frac{\partial z}{\partial T}$ based on the surface cooling and monthly ocean temperature at each TC location (Li et al., 2016). Q is calculated at each grid box and then summed over a fixed domain of 6° × 6° to account for nonuniform mixing. The global ocean heat uptake (OHU) rate induced by TCs is derived for each year. By taking F to be 0.55, the OHU rate was estimated to be ~0.11 PW by Li et al. (2016). We follow their method and obtain a similar estimate of 0.13 ± 0.02 PW.

Note that Li et al. (2016) employed a footprint method to estimate OHU rate using a fixed domain of 6° × 6°. In contrast, we sum Q within the varying ROI boundary. By so doing, we are able to capture the varying asymmetry and size of cold wakes. The OHU rate is estimated to be 0.48 ± 0.10 PW, ~3.7 times of the estimate of Li et al. (2016). The larger estimate using the ROI method might result from the larger cold wake area determined. Note that the mean rROI is 487 km, much larger than the equivalent cold wake size (~333 km) of a fixed 6° × 6° domain. Since this method depends on the ROI boundary, it is sensitive to the parameters used in the ROI method. For example, the spatial filter can alter the estimates by up to 20% (Table S1) while the impact of the tolerance distance is negligible (Table S2). Other details might also contribute to the difference in the estimation, such as time intervals or mesoscale eddy filters in determining the cold wakes, and different ocean reanalysis data used for the calculation of dh. Nonetheless, the OHU cannot be reliably estimated without the consideration of varying cold wake sizes.

The estimate above may overestimate OHU, especially for those slow-moving or stalled storms due to double counting (R. Sriver, personal communication). One advantage of the ROI method is that the overlapping area between the two consecutive cold wake regions can be reliably determined, which is hard to achieve in traditional footprint method. We discarded the overlapped area possessing the smaller OHU because it is the accumulative OHU matters. The OHU rate after accounting for the double-counting problem reduced to 0.20 ± 0.05 PW, ~42% of the original estimate. Similar OHU rates (~0.20 PW; Tables S1 and S2) are found after accounting for the double-counting problem for the uncertainties involved in the ROI method (Text S3). This suggests that OHU estimate can be significantly overestimated without the consideration of double counting. The estimates in this study is smaller than that (0.32 ± 0.15 PW) based on a different approach using sea surface height data by Mei et al. (2013), but generally within the uncertainty range noted in previous studies (Emanuel, 2001; Jansen et al., 2010; Li et al., 2016; Mei et al., 2013; Sriver et al., 2008).

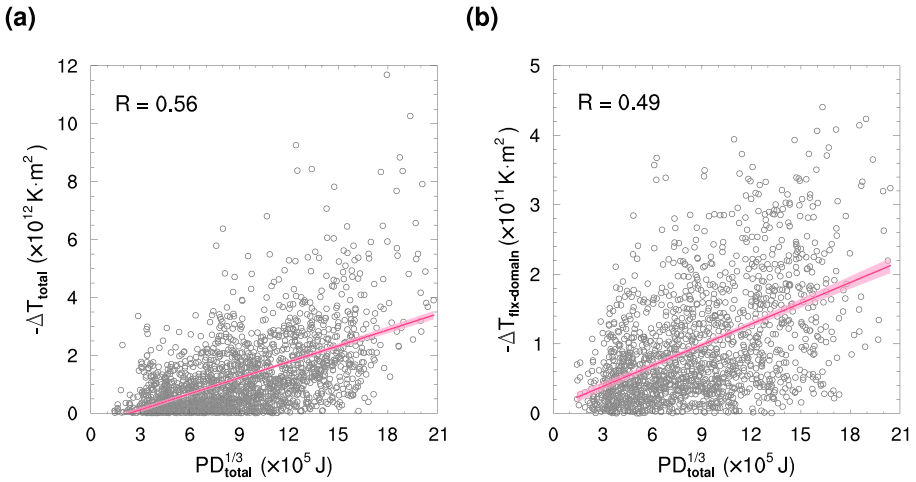

Figure 4. (a) Scatterplot between TC-induced total cooling (ΔT_{total}; K·m^2) and the cube root of total power dissipation ($PD_{total}^{1/3}$; J) of TCs. (b) Same as (a) but between the local cooling ($\Delta T_{fix\ -\ domain}$; K·m^2) and the cube root of total power dissipation ($PD_{total}^{1/3}$; J). Linear regression fits are denoted as dark pink lines with two-sided 95% confidence bounds of the slopes shaded in pink. Correlation coefficients are shown in the top left corners, respectively.

4. Conclusions and Discussion

In this study, we derived the size of TC-induced cold wakes by applying two objective methods to daily SST fields. The cold wake size is found to correlate reasonably well with the size of the TC wind field derived from the QuikSCAT-R database, suggesting the potential usage of cold wake size to infer TC wind field size and vice versa. We further present two applications for the new size metrics. Our quantification of TC-induced total cooling considers both the magnitude and size of the cooling. The total cooling better captures the total TC power dissipation than the local cooling used in previous studies. Meanwhile, TC-induced ocean heat uptake estimated considering varying cold wake sizes is 0.48 ± 0.10 PW, larger than the estimate assuming a fixed cold wake size. Furthermore, this estimate is reduced to 0.20 ± 0.05 PW after considering the double-counting problem. Note that the uncertainty involved in these estimates can be large (20–25% for the parameters tested in the study). Double-counting problem can be well addressed using the ROI method since the cold wake boundary and their overlapping area can be well quantified. Although a more accurate estimate is hampered by the limitation of temperature profiles without considering thermocline seasonal variations (Jansen et al., 2010), it highlights the important role of cold wake size in such estimates.

We hope this study as a starting point to shed light on the potential impact of TC size on the interactions between TCs and their environment. For example, the conventional estimates of TCs' climatological effect, such as TC accumulated energy and power dissipation, have rarely considered variations in TC size, although these variations might make a significant contribution. Moreover, the influence of TC size on TC intensity evolution is underexplored. An interesting issue inspired by this work is to incorporate the information of TC size in parameterizing the effect of TC-generated cold wakes. This will help to more accurately include the effect of the negative SST feedback in TC simulations without being coupled to an ocean model. These topics warrant further investigation.

Acknowledgments
AcknowledgementsThis work was supported by the National Natural Science Foundation of China (41775098) and Tsinghua University Initiative Scientific Research Program (2019Z07L01001). We are grateful for the discussion with Ryan Sriver regarding ocean heat uptake calculations. We gratefully thank the groups of IBTrACS (https://www.ncdc.noaa.gov/ibtracs/index.php), Optimum Interpolation Sea Surface Temperature (https://www.ncdc.noaa.gov/oisst), QuikSCAT-R (https://verif.rap.ucar.edu/tcdata/quikscat/), and CCMP (http://www.remss.com/measurements/ccmp/) for providing public access to various data sets. Cold wake size data are available at https://github.com/yanluan-thu/tc-mixing.

References

Atlas, R., Hoffman, R. N., Ardizzone, J., Leidner, S. M., Jusem, J. C., Smith, D. K., & Gombos, D. (2011). A cross-calibrated, multiplatform ocean surface wind velocity product for meteorological and oceanographic applications. *Bulletin of the American Meteorological Society*, *92*(2), 157–174. https://doi.org/10.1175/2010BAMS2946.1

Carrasco, C. A., Landsea, C. W., & Lin, Y.-L. (2014). The influence of tropical cyclone size on its intensification. *Weather and Forecasting*, *29*(3), 582–590. https://doi.org/10.1175/WAF-D-13-00092.1

Chavas, D., Yonekura, E., Karamperidou, C., Cavanaugh, N., & Serafin, K. (2013). U.S. hurricanes and economic damage: Extreme value perspective. *Natural Hazards Review*, *14*(4), 237–246. https://doi.org/10.1061/(ASCE)NH.1527-6996.0000102

Chavas, D. R., & Emanuel, K. A. (2010). A QuikSCAT climatology of tropical cyclone size. *Geophysical Research Letters*, *37*, L18816. https://doi.org/10.1029/2010GL044558

Chavas, D. R., Lin, N., Dong, W., & Lin, Y. (2016). Observed tropical cyclone size revisited. *Journal of Climate*, *29*(8), 2923–2939. https://doi.org/10.1175/JCLI-D-15-0731.1

Chelton, D. B., Schlax, M. G., Samelson, R. M., & de Szoeke, R. A. (2007). Global observations of large oceanic eddies. *Geophysical Research Letters*, *34*, L15606. https://doi.org/10.1029/2007GL030812

Dare, R. A., & McBride, J. L. (2011). Sea surface temperature response to tropical cyclones. *Monthly Weather Review*, *139*(12), 3798–3808. https://doi.org/10.1175/Mwr-D-10-05019.1

de Boyer Montégut, C. (2004). Mixed layer depth over the global ocean: An examination of profile data and a profile-based climatology. *Journal of Geophysical Research*, *109*, C12003. https://doi.org/10.1029/2004JC002378

Emanuel, K. (2001). Contribution of tropical cyclones to meridional heat transport by the oceans. *Journal of Geophysical Research*, *106*(D14), 14,771–14,781. https://doi.org/10.1029/2000JD900641

Emanuel, K. (2005). Increasing destructiveness of tropical cyclones over the past 30 years. *Nature*, *436*(7051), 686–688. https://doi.org/10.1038/nature03906

Fedorov, A. V., Brierley, C. M., & Emanuel, K. (2010). Tropical cyclones and permanent El Niño in the early Pliocene epoch. *Nature*, *463*(7284), 1066–1070. https://doi.org/10.1038/nature08831

Guo, X., & Tan, Z. M. (2017). Tropical cyclone fullness: A new concept for interpreting storm intensity. *Geophysical Research Letters*, *44*, 4324–4331. https://doi.org/10.1002/2017GL073680

Holland, G. J. (1980). An analytic model of the wind and pressure profiles in hurricanes. *Monthly Weather Review*, *108*(8), 1212–1218. https://doi.org/10.1175/1520-0493(1980)108<1212:aamotw>2.0.co;2

Jansen, M. F., Ferrari, R., & Mooring, T. A. (2010). Seasonal versus permanent thermocline warming by tropical cyclones. *Geophysical Research Letters*, *37*, L03602. https://doi.org/10.1029/2009GL041808

Kimball, S. K., & Mulekar, M. S. (2004). A 15-year climatology of North Atlantic tropical cyclones. Part I: Size parameters. *Journal of Climate*, *17*(18), 3555–3575. https://doi.org/10.1175/1520-0442(2004)017<3555:AYCONA>2.0.CO;2

Knaff, J. A., Longmore, S. P., & Molenar, D. A. (2014). An objective satellite-based tropical cyclone size climatology. *Journal of Climate*, *27*(1), 455–476. https://doi.org/10.1175/Jcli-D-13-00096.1

Knaff, J. A., Sampson, C. R., DeMaria, M., Marchok, T. P., Gross, J. M., & McAdie, C. J. (2007). Statistical tropical cyclone wind radii prediction using climatology and persistence. *Weather and Forecasting*, *22*(4), 781–791. https://doi.org/10.1175/WAF1026.1

Knapp, K. R., Kruk, M. C., Levinson, D. H., Diamond, H. J., & Neumann, C. J. (2010). The International Best Track Archive for Climate Stewardship (IBTrACS). *Bulletin of the American Meteorological Society*, *91*(3), 363–376. https://doi.org/10.1175/2009bams2755.1

Knutson, T. R., Sirutis, J. J., Zhao, M., Tuleya, R. E., Bender, M., Vecchi, G. A., et al. (2015). Global projections of intense tropical cyclone activity for the late twenty-first century from dynamical downscaling of CMIP5/RCP4.5 scenarios. *Journal of Climate*, *28*(18), 7203–7224. https://doi.org/10.1175/JCLI-D-15-0129.1

Li, H., Sriver, R. L., & Goes, M. (2016). Modeled sensitivity of the Northwestern Pacific upper-ocean response to tropical cyclones in a fully coupled climate model with varying ocean grid resolution. *Journal of Geophysical Research: Oceans*, *121*, 586–601. https://doi.org/10.1002/2015JC011226

Lin, N., & Chavas, D. (2012). On hurricane parametric wind and applications in storm surge modeling. *Journal of Geophysical Research*, *117*, D09120. https://doi.org/10.1029/2011JD017126

Lin, Y., Zhao, M., & Zhang, M. (2015). Tropical cyclone rainfall area controlled by relative sea surface temperature. *Nature Communications*, *6*(1), 6591. https://doi.org/10.1038/ncomms7591

Lloyd, I. D., & Vecchi, G. A. (2011). Observational evidence for oceanic controls on hurricane intensity. *Journal of Climate*, *24*(4), 1138–1153 . https://doi.org/10.1175/2010jcli3763.1

Mei, W., & Pasquero, C. (2012). Restratification of the upper ocean after the passage of a tropical cyclone: A numerical study. *Journal of Physical Oceanography*, *42*(9), 1377–1401. https://doi.org/10.1175/jpo-d-11-0209.1

Mei, W., & Pasquero, C. (2013). Spatial and temporal characterization of sea surface temperature response to tropical cyclones*. *Journal of Climate*, *26*(11), 3745–3765. https://doi.org/10.1175/JCLI-D-12-00125.1

Mei, W., Primeau, F., McWilliams, J. C., & Pasquero, C. (2013). Sea surface height evidence for long-term warming effects of tropical cyclones on the ocean. *Proceedings of the National Academy of Sciences of the United States of America*, *110*(38), 15,207–15,210. https://doi.org/10.1073/pnas.1306753110

Merrill, R. T. (1984). A comparison of large and small tropical cyclones. *Monthly Weather Review*, *112*(7), 1408–1418. https://doi.org/10.1175/1520-0493(1984)112<1408:Acolas>2.0.Co;2

Park, J. J., Kwon, Y.-O., & Price, J. F. (2011). Argo array observation of ocean heat content changes induced by tropical cyclones in the North Pacific. *Journal of Geophysical Research*, *116*, C12025. https://doi.org/10.1029/2011JC007165

Pasquero, C., & Emanuel, K. (2008). Tropical cyclones and transient upper-ocean warming. *Journal of Climate*, *21*(1), 149–162. https://doi.org/10.1175/2007JCLI1550.1

Price, J. F. (1981). Upper ocean response to a hurricane. *Journal of Physical Oceanography*, *11*(2), 153–175. https://doi.org/10.1175/1520-0485(1981)011<0153:UORTAH>2.0.CO;2

Reynolds, R. W., Smith, T. M., Liu, C., Chelton, D. B., Casey, K. S., & Schlax, M. G. (2007). Daily high-resolution-blended analyses for sea surface temperature. *Journal of Climate*, *20*(22), 5473–5496. https://doi.org/10.1175/2007jcli1824.1

Ricciardulli, L., & Wentz, F. J. (2015). A scatterometer geophysical model function for climate-quality winds: QuikSCAT Ku-2011. *Journal of Atmospheric and Oceanic Technology*, *32*(10), 1829–1846. https://doi.org/10.1175/JTECH-D-15-0008.1

Sriver, R. L., Goes, M., Mann, M. E., & Keller, K. (2010). Climate response to tropical cyclone-induced ocean mixing in an Earth system model of intermediate complexity. *Journal of Geophysical Research*, *115*, C10042. https://doi.org/10.1029/2010JC006106

Sriver, R. L., & Huber, M. (2007). Observational evidence for an ocean heat pump induced by tropical cyclones. *Nature*, *447*(7144), 577–580. https://doi.org/10.1038/nature05785

Sriver, R. L., Huber, M., & Nusbaumer, J. (2008). Investigating tropical cyclone-climate feedbacks using the TRMM Microwave Imager and the Quick Scatterometer. *Geochemistry, Geophysics, Geosystems*, *9*, Q09V11. https://doi.org/10.1029/2007GC001842

Sun, J., Oey, L.-Y., Chang, R., Xu, F., & Huang, S.-M. (2015). Ocean response to typhoon Nuri (2008) in western Pacific and South China Sea. *Ocean Dynamics*, *65*(5), 735–749. https://doi.org/10.1007/s10236-015-0823-0

Vincent, E. M., Lengaigne, M., Madec, G., Vialard, J., Samson, G., Jourdain, N. C., et al. (2012). Processes setting the characteristics of sea surface cooling induced by tropical cyclones. *Journal of Geophysical Research*, *117*, C02020. https://doi.org/10.1029/2011JC007396

Vincent, E. M., Lengaigne, M., Vialard, J., Madec, G., Jourdain, N. C., & Masson, S. (2012). Assessing the oceanic control on the amplitude of sea surface cooling induced by tropical cyclones. *Journal of Geophysical Research*, *117*, C05023. https://doi.org/10.1029/2011JC007705

Wang, G., Wu, L., Johnson, N. C., & Ling, Z. (2016). Observed three-dimensional structure of ocean cooling induced by Pacific tropical cyclones. *Geophysical Research Letters*, *43*, 7632–7638. https://doi.org/10.1002/2016GL069605

Xu, J., & Wang, Y. (2015). A statistical analysis on the dependence of tropical cyclone intensification rate on the storm intensity and size in the North Atlantic. *Weather and Forecasting*, *30*(3), 692–701. https://doi.org/10.1175/WAF-D-14-00141.1

Zhang, L., & Oey, L. (2018). An observational analysis of ocean surface waves in tropical cyclones in the western North Pacific Ocean. *Journal of Geophysical Research: Oceans*, *124*, 184–195. https://doi.org/10.1029/2018JC014517

Zhang, S., Harrison, M. J., Rosati, A., & Wittenberg, A. (2007). System design and evaluation of coupled ensemble data assimilation for global oceanic climate studies. *Monthly Weather Review*, *135*(10), 3541–3564. https://doi.org/10.1175/MWR3466.1

Erratum

In the originally published version of this article, the legends of Figures 2 and 3 were switched. This error has since been corrected, and the present version may be considered the authoritative version of record.